Non-Epitaxial Gold-Tipped ZnSe Hybrid Nanorods for Efficient Photocatalytic Hydrogen Production

Wei Chen[a], Xiaojie Li[b], Fei Wang[a], Shaghraf Javaid[a], Yingping Pang[a], Jiayi Chen[a], Zongyou Yin[c],Shaobin Wang[b], Yunguo Li[d]* and Guohua Jia[a]**

W. Chen, F. Wang, S. Javaid, Y. Pang, J. Chen and Dr. G. Jia
Curtin Institute of Functional Molecules and Interfaces, School of Molecular and Life Sciences
Curtin University, Bentley, Perth WA, 6102, Australia
E-mail: guohua.jia@curtin.edu.au

X. Li, Prof. S. Wang
Department of Chemical Engineering
Curtin University, Bentley, Perth WA, 6102, Australia
School of Chemical Engineering, The University of Adelaide, Adelaide SA 5005, Australia
E-mail: shaobin.wang@adelaide.edu.au

Dr. Z. Yin
Research School of Chemistry, The Australian National University, Canberra, Australian Capital Territory 2601, Australia

Dr. Y. Li
Faculty of Mathematical and Physical Sciences, University College London, Gower Street, London WC1E 6BT, United Kingdom
E-mail: yunguo.li@ucl.ac.uk

Keywords: Au-ZnSe, hybrid nanorods, cadmium-free, hydrogen production, photocatalysis

Abstract: For the first time, colloidal gold (Au)-ZnSe hybrid nanorods (NRs) with controlled size and location of Au domains are synthesized and used for hydrogen production by photocatalytic water splitting. Au tips were found to grow on the apices of ZnSe NRs non-epitaxially to form an interface with no preference of orientation between Au (111) and ZnSe (001). Density functional theory (DFT) calculations reveal that the Au tips on ZnSe hybrid NRs gain enhanced adsorption of H compared to pristine Au, which favors the hydrogen evolution reaction. Photocatalytic tests reveal that the Au tips on ZnSe NRs effectively enhance the photocatalytic performance in hydrogen generation, in which the single Au-tipped ZnSe hybrid NRs show the highest photocatalytic hydrogen production rate of 437.8 $\mu mol \cdot h^{-1} \cdot g^{-1}$ in comparison with a rate of 51.5 $\mu mol \cdot h^{-1} \cdot g^{-1}$ for pristine ZnSe NRs. An

apparent quantum efficiency of 1.3% for hydrogen evolution reaction for single Au-tipped ZnSe hybrid NRs was obtained, showing the potential application of this type of cadmium (Cd)-free metal-semiconductor hybrid NPs in solar hydrogen production. This work opens an avenue towards Cd-free hybrid nanoparticle (NP)-based photocatalysis for clean fuel production.

1. Introduction

Metal-semiconductor hybrid NPs integrating multiple components into a single nano-object at the nanoscale have received tremendous attention in recent years because they not only possess the properties of individual components but also manifest a synergistic behaviour stemming from the materials interaction.[1-8] This makes the metal-semiconductor hybrid NPs promising in a wide scope of applications ranging from photo-catalysis for hydrogen generation or CO_2 reduction,[9-11] photodynamic therapy,[12,13] wound healing,[14,15] to photoinitiators for 3D printing.[16]

Among these materials, metal-semiconductor NRs, such as Au-CdSe,[17] Pt-CdSe,[18] Au-CdS,[19] Pt-CdS, and Pt-CdSe/CdS[20] are of particular interest. This is because that the hybrid NPs with one-dimensional shape enable more efficient charge separation ability in comparison with hybrid NPs of other morphologies.[20] The noble metal component within the hybrid NPs can work as a co-catalyst by providing the surface active sites for catalytic reaction with a lower activation energy barrier than semiconductors only.[21-23] The lifetime of charge carriers in these materials is also extended because of the enhanced rate of electron-hole separation.[24] Owing to the effective light-induced electron-hole separation, noble metal-semiconductor hybrid NRs such as Pt-CdS,[25] Pd-CdSe@CdS-Au,[26] CdSe/CdS-Pt[20,23] and CdSe/CdS-Pt-Au[27] have been extensively studied in photo-catalytic water splitting for hydrogen production. Besides hydrogen evolution, CdS nanocrystals with a dinuclear cobalt

catalyst[11] or CdS ((Mo-Bi)S_x/CdS)[28] can be used for the selective photocatalytic CO_2 reduction.

Up to now, the research into metal-semiconductor hybrid NRs is mainly focused on Cd-based systems due to the mature synthetic protocols on the precise control of size, shape, composition and metal location and their good performances in photocatalysis.[1,3,4,9,29] However, the high toxicity and the carcinogenicity of Cd-based materials is the main obstacle that restricts their widespread applications.[30,31] Compared with Cd-based materials, Zn-based semiconductor nanocrystals are less or non-toxic and environmental-friendly. Meanwhile, due to the wide band gap of Zn-based II-VI semiconductors (bulk ZnSe: 2.82 eV; bulk ZnS 3.7 eV), these NPs absorb near ultraviolet (UV) and blue light from solar spectrum, unlike the traditional Cd-based nanocrystals absorbing visible light. Given the main purpose for this project is to investigate the positional tipping effect from Au onto ZnSe nanorods on photocatalysis, the complementary absorption of longer wavelength photons to maximize solar harvesting for photocatalysis enhancement is expectable by heterojunction and doping strategies.[32,33] These merits make them potential supplements or alternatives to the Cd-based materials in photocatalytic hydrogen generation and biomedical applications[12]. Recent research on ZnSe and alloyed ZnSeS NRs indicated that these Cd-free NRs can be adopted as efficient photocatalysts for efficient hydrogen generation and oxygen evolution reactions.[34,35]

Metal-ZnSe hybrid NRs have been rarely reported due to the difficulties in the synthesis of ZnSe NRs.[36] To the best of our knowledge, the catalytic properties of these hybrid nanostructures have not been previously investigated. Pradhan *et al.* reported Au tipped wormlike ZnSe hybrid NPs through the growth of a heteroepitaxial junction between cubic Au and zinc blende ZnSe at elevated temperatures.[37] However, the Au-ZnSe hybrids obtained by a wet-chemical approach are not uniform after annealing at a high temperature of 250 ^{o}C, which deteriorates their optical and catalytic properties as these properties are closely relevant to the size, shape and spacial distribution of the metal-semiconductor hybrid NPs.

Further studies into the precise control on the size, shape and phase of this new type of Au-ZnSe hybrid NPs, especially NRs, and their catalytic properties are highly demanded and important.

Herein, for the first time, we use a wet-chemical method to obtain Au-ZnSe hybrid NRs with controlled size and location of Au domains on ZnSe NRs. The precisely selective growth of Au tips on the apices of ZnSe NRs was achieved and this new Cd-free metal-semiconductor hybrid NRs has been demonstrated as excellent photocatalyts for hydrogen generation through water splitting, which are comparable with Cd-based hybrid NPs.

2. Results and Discussion

2.1. Synthesis and Characterization of Au-ZnSe Hybrid NRs

Firstly, ZnSe NRs were synthesized by a heat-up method according to a previously reported method with some modifications[38] (See Experimental Section in the Supporting Information). In a typical synthesis, zinc acetate and selenium powder were employed as the precursors while oleylamine and 1-dodecanethiol (DDT) were used as the ligand and solvent, respectively, to synthesize ZnSe NRs at 260 ℃ using standard Schleck techniques.

Transmission electron microscope (TEM) image (Figure S1) confirms the particles are elongated NRs. The histograms of size distribution show that the length and diameter of the synthesized ZnSe NRs are 24.8 ± 7.7 nm and 2.1 ± 0.3 nm, respectively (Figure S2). As DDT may act as a S source in the synthesis, powder X-ray diffraction (XRD) (Figure S3), high resolution TEM (HRTEM) (Figure S4), UV-Vis absorption (Figure S5), X-ray photoelectron spectroscopy (XPS) (Figure S6) and scanning TEM (STEM)-energy-dispersive X-ray spectroscopy (EDS) (Figure S7) were conducted to verify the composition and crystal phase of the obtained NRs in order to elucidate the sulfur incorporation in ZnSe NRs during their growth. The XRD pattern (Figure S3) matches well with the standard wurtzite ZnSe and no shift of the diffraction peaks is observed with respect to those of the standard wurtzite ZnSe,

confirming the pure phase of wurtzite ZnSe NRs. The sharp peak of the (002) plane corroborates the orientation of the long axis of wurtzite ZnSe NRs. The distance of lattice plane extracted by fast Fourier transform (FFT) analysis of HRTEM is shown in Figure S4 and Table S1 to further identify the crystal structure and composition of synthesized NRs. As seen from Figure S4 and Table S1**,** the lattice distance and angles between planes of synthesized NRs matches the (100), (002), (101) and $(10\bar{1})$ of wurtzite ZnSe structure well, which further proved the composition and structure of ZnSe NRs rather than alloyed ZnSeS. The absorption of synthesized NRs with a diameter of 2.1 ± 0.3 nm (Figure S5) showed an absorption peak at 368 nm which is in accordance of the excitonic peak of ZnSe with this size. The XPS spectrum of ZnSe NRs synthesized in this work was shown in Figure S6. As seen from Figure S6, the Zn element presents solely as Zn(+2). As for S 2p, it has closely spaced spin-orbit components (Δ=1.16 eV, intensity ratio=0.511) which overlap with those of Se 3p. The XPS spectrum of ZnSe NRs synthesized using dodecanethiol and oleylamine as the surfactant/solvents in this work was dominated by two peaks at 160.3 eV and 166.0 eV, which can be assigned to Se $3p_{3/2}$ and Se $3p_{5/2}$, respectively.[38] The other two weak peaks positioned at 162.4 eV and 163.5 eV correspond to the typical value of metal-thiol binding energy of S 2p.[38]

Element mapping of ZnSe NRs was also conducted to further verify their composition (Figure S7)**.** EDS mapping of Zn and Se of the obtained ZnSe nanorods shows that Zn and Se elements are distributed evenly throughout the NPs. A weak signal corresponding to S element is also detected on the NPs and the surrounding background. The presence of the S signal can be attributed to the dodecanethiol ligands binding on the surface of the ZnSe NRs and amorphous carbon film, consistent with the results of XPS measurements. Based on the above characterization results, we confirmed that the synthesized nanorods are ZnSe rather than alloyed $ZnSe_xS_{1-x}$ structure, although there might be some thiol ligand binding on

nanorods surface and etching could bring in a little bit of S to ZnSe NRs. Thus the main composition should be ZnSe. After the synthesis, the obtained ZnSe NRs were collected, purified and further used to grow Au tips toward Au-ZnSe hybrid NRs.

For Au tips growth on ZnSe NRs, we employed $AuCl_3$ as a gold precursor and dodecylamine as both surfactant and reductant in toluene solution for preparation at room temperature.[18] Typically $AuCl_3$ was firstly dissolved with dodecylamine in toluene by sonication and kept as Au stock solution, and then a predetermined volume of the Au stock solution was injected into ZnSe NRs dispersed in toluene under N_2 protection. The Au tips were allowed for growth for a certain time at room temperature before quenched by addition of acetone. (see Experimental Section in Supporting Information for details).

UV-Vis absorption spectroscopy was carried out to monitor the growth of Au on the ZnSe NRs and to investigate the optical properties (**Figure 1**). At a low molar ratio of Au precursor to ZnSe NRs (127:1) (Sample 1 in Figure 1), the final solution is colourless. The absorption spectrum of sample 1 also shows a distinct excitonic peak at 368 nm which is similar to that of the original ZnSe NRs (Figure S5). With an increased molar ratio of Au precursor to ZnSe NRs (254:1 to 1270:1, samples 2-4 in Figure 1), the absorption exciton peaks of ZnSe NRs become broader and a tail at the longer wavelength appears and gradually becomes prominent. Meanwhile, the color of the product solutions gradually change from light yellow to dark brown. These observations indicate the modified electronic structure of Au-ZnSe hybrid NRs rather than the simple mixture of ZnSe semiconductor and metal tips.[2]

The absorption spectra of sample 2-4 present broad features with the tails extending to the low energy region of the spectra. The mixing of the electronic states of metal and semiconductors in hybrid NRs may result in the strong scattering in their absorption spectra, which is previously observed in metal-CdS (CdSe) hybrid NRs. The decreased solubility of Au-ZnSe hybrid NRs after the growth of the Au tips may also enhance the scattering of the absorption spectra.[39]

TEM measurements were conducted to verify the growth of Au on ZnSe NRs. **Figure 2** shows TEM and high-angle annular dark-field-STEM (HAADF-STEM) images of Au-ZnSe hybrid NRs with Au tips at variable sizes. At a low molar ratio of Au precursor to ZnSe NRs (127:1) for the growth of 1 hour, almost no gold was grown on ZnSe NRs (Figure S8a), which is consistent with the observation that the excitonic peak in UV-Vis absorption spectrum of this sample keeps almost the same as that of the original ZnSe NRs (Figure S5). When more Au precursor was used for growth (n($AuCl_3$:ZnSe NRs)=254:1), very small gold tips (Dark spots in Figure 2a, bright spots in Figure 2d) with a diameter of 1.3 ± 0.2 nm (Figure 2g) grew onto one of the two apices of the ZnSe NRs. This observation is similar to the Au growth on CdSe NRs reported by Mokari and co-workers in which single Au tip growth is dominant at the low molar ratio of Au to NRs.[40] A further increase of the molar ratio of $AuCl_3$ to ZnSe NRs to 762:1 (Figure 2b, 2e) leads to more growth of Au tips. The diameter of the Au tips increases to 1.6 ± 0.3 nm (Figure 2h) and apparently the Au tips grew on both apices of the majority of ZnSe NRs. When the molar ratio of $AuCl_3$ to ZnSe NRs was increased to 1270:1 (Figure 2c, 2f), larger gold tips with a diameter of 2.2 ± 0.3 nm (Figure 2i) grew on both apices of ZnSe NRs. In some cases, Au growth on the body of ZnSe NRs was also observed (Figure 2c, 2f), which can be attributed to the defect-induced growth of Au on the NRs.

The above observations suggested site-selective growth of Au on different facets of the one-dimensional anisotropic wurtzite ZnSe NRs, attributing to the higher reactivity of the end facets with increased surface energy and the imperfect ligand passivation, which is similar to other systems such as Au-CdSe[2] and Au-CdSe/CdS.[40] In other words, there are large differences in surface energy between the side facets of (100) and the end facets of (002) of wurtzite ZnSe NRs.[8] The (002) planes are alternately composed of either Zn or Se atoms, which makes Au growth at earlier stages more favourable on the Se rich facets in single Au tip ZnSe hybrid NRs.[3] Another important factor influencing Au growth is the sparse ligand

coverage of the apex region of the NRs with respect to their body.[41] When more Au precursor was used for growth, the increased supersaturation of monomers may overcome the energy barrier that required for the gold growth on ZnSe NRs. Furthermore, when excessive amount of Au precursor was used (n($AuCl_3$:ZnSe NRs)=2540:1), agglomeration of Au tips can be found (Figure S7b). The Au-ZnSe hybrid NRs with large Au tips may be attributed to the ripening process as the reaction was performed for a prolonged time with low monomer concentrations.[39]

STEM-EDS elemental mapping was used to analyze the composition and distribution of the hybrid NRs. Zn and Se elements are distributed evenly throughout the ZnSe NRs (Figure S9). Although the location of Au cannot be easily recognized from EDS mapping data, the large contrast of Au with respect to ZnSe in STEM images confirms the Au (brighter spots in STEM images in Figure 2d-e) growth on the apices of ZnSe NRs.

Figure 3a presents the XRD pattern of Au-ZnSe hybrid NRs. The main diffraction peaks can be indexed to the (100), (002) and (110) of the hexagonal wurtzite ZnSe (JCPDS card #80-0008), while the other diffraction peaks can be assigned to the (111), (200) and (511) of the face-centered cubic (FCC) Au tips (JCPDS card #99-0056). HRTEM and the associated FFT analysis were used to further reveal the crystal structure of Au tips (Figure 3b). The lattice plane spacings of 0.235 nm and 0.204 nm agree well with the (111) and (200) lattice planes of cubic Au, respectively (Figure 3b). It is noted that, due to the considerable mass difference among Au, Zn and Se atoms, ZnSe NRs are hard to be visualized at a high magnification while the lattice of Au nanocrystals can be clearly observed. The HRTEM images confirmed that Au tips on ZnSe hybrid NRs are face-centered cubic structure (inset in Figure 3b), which is consistent with the XRD results.

TEM, HRTEM, STEM-EDS and XRD characterizations have confirmed the successful growth of cubic phase Au tips on wurtzite ZnSe NRs. We further employed high-resolution XPS to examine the binding environments in the Au-ZnSe hybrid NRs. The survey spectrum of the sample reveals the binding energies for Zn 2p, Se 3d, and Au 3d (**Figure 4**a). The main binding energy peaks at ~84 eV and ~87.7 eV of the high resolution XPS spectrum of Au are attributed to Au(0) $4f_{7/2}$ and $4f_{5/2}$ (Figure 4b), respectively.[42]

The distinct peaks observed at higher energy such as ~84.9 eV and ~88.6 eV can be assigned to $4f_{7/2}$ and $4f_{5/2}$ binding energy peaks of Au(+1).[43] Although the majority of the $AuCl_3$ precursor has been reduced to Au(0), there may be still a small portion of Au^+ not completely reduced to Au (0) under a mild reducing condition. Figure 4c shows two XPS peaks at around 54.3 eV and 55.2 eV, corresponding to the binding energies of Se 3d.[44] A small broaden peak at 59.5 eV indicated a small proportion of SeO_2 impurity formed due to partial oxidation of Se at the surface of the NRs.[8, 45] The two Zn 2p peaks at 1045 eV and 1022 eV in Figure 4d correspond to Zn $2p_{1/2}$ and $2p_{3/2}$, respectively, which confirm the presence of Zn(+2).[46]

2.2. Au growth orientation on ZnSe NRs

Based on the above results, we found that Au tips preferentially grow on the Se-rich apex of ZnSe NRs, and then on both apices. To further reveal the growth mechanism of Au-tipped ZnSe hybrid NRs, we analyzed their HRTEM images to determine if the Au tips grow epitaxially onto the apices of the ZnSe NRs. As the predominant lattice planes for Au tips and ZnSe NRs within the Au-ZnSe hybrid NRs are the (111) and (002), respectively, we specifically measured the angles between these two planes to see if there is a fixed angle between them. As confirmed by the XRD pattern and HRTEM image, the (002) plane is perpendicular to the *c*-axis of the wurtzite ZnSe NRs. As for the Au tips with the cubic structure, the (111) plane can easily be identified in the HRTEM images. So we measured the

angle between the (111) plane of Au tips and the length direction of ZnSe NRs, which corresponds to the angle between the (111) plane of Au tips and the (100) plane of ZnSe NRs. Because of the small size of Au tips and the large contrast between ZnSe rods and Au tips, it is difficult to clearly resolve both the lattice planes simultaneously. However, we could verify the length direction of the ZnSe NRs and the (111) plane of Au tips at different magnifications.

The schematic of the angle measurement is shown in Figure S10. Statistics on the angles between the length direction of the ZnSe NRs and the (111) planes of Au tips of 28 Au-ZnSe hybrid NRs is shown in Figure S10c. If epitaxial growth does occur for this system, we would expect to see a set of discrete, well-defined angles between these sets of lattice planes. For example, from geometrical considerations, if Au (111) aligned with ZnSe (002), the angle between the Au (111) and ZnSe (100) will be 90°. However, statistics show that the angle between Au (111) facet and ZnSe (100) facet of NRs varied between 0° to 90° (Figure S10c), indicating that gold was randomly growth on ZnSe NRs without preferable orientation. Thus, we conclude that the growth of Au tips on wurtzite ZnSe NRs is nonepitaxial.

This finding is different from the reports of Pradhan *et al.* that the formation of the heteroepitaxial junction of the (111) facet of cubic Au on the (111) facet of wormlike zinc blend ZnSe nanocrystals, as well as the epitaxial growth of the (111) facet of gold along the [002] direction of the CdSe NRs.[37,47] In both cases, Au precursor was injected into the pre-synthesized zinc blende ZnSe or wurtzite CdSe nanocrystals at a high temperature of ~190 ℃ and grew at 250 ℃. Another work by Manna and co-workers[17, 19] reveals that annealing of non-epitaxial Au-CdS nanocrystals prepared by wet-chemical synthetic approaches results in the formation of epitaxial Au-CdS hybrid nanocrystals. It is evident that a high temperature is essential for the formation of epitexial Au-semiconductor hybrid nanocrystals while the kinetically controlled wet-chemical synthetic routes at room temperature will generate non-epitaxial Au-ZnSe hybrid NRs.

2.3. Density functional theory (DFT) simulations of Au growth

To further establish the proposed non-epitaxial growth mechanism and in particular to elucidate no preferential epitaxial relationship between gold metal and ZnSe domain, we employed the first-principles methods based on DFT to investigate the potential energy surface of ZnSe(001)/Au(111) interface (see details in Supporting Information). Although the HRTEM measurements suggest no preference of a specific orientation relationship between Au and ZnSe, we think the interface between the Au (111) and ZnSe (001) is a typical and representative structure of the hybrid system, as it is composed of the most closely packed planes and resembles the Au-CdSe hybrid system. We calculated the potential energy surface (PES) of interfacing ZnSe (001) and Au (111) (see Supporting Information). The initial input structure and calculated PES are displayed in **Figure 5**a and 5b, respectively. The highest barrier between energy minima is 0.1 eV per Au atom at the interface layer. It can be inferred that the barrier can work at low temperatures like room temperature to induce non-epitaxial growth of Au on the ZnSe (001) surface. At elevated temperatures the small barrier may be overcome and the growth of epitaxial Au or transition into epitaxial Au can be seen.

We then further explored the detailed atomic interface structure. The ZnSe(001)/Au(111) interface structure with the minimum energy was chosen for further studies and relaxed with a Monkhorst-Pack **k**-point set of 2×2×1. Seven Au atoms at the interface layer that are most distant from ZnSe lattice sites were removed to create a ZnSe(001)/Zn_0Au_1/Au(111) interface, namely, an interface with the top layer Zn atoms completely substituted by the interfacing Au layer atoms and no more Au left in the interfacing Au single layer. From the ZnSe(001)/Zn_0Au_1/Au(111) interface, we varied the ratio of Zn to Au at the interfacing single layer to obtain the ZnSe(001)/$Zn_{1/3}Au_{2/3}$/Au(111), ZnSe(001)/$Zn_{2/3}Au_{1/3}$/Au(111), and ZnSe(001)/Zn_1Au_0/Au(111) structures. The phase diagram of the interface can be obtained and is plotted in Figure 5c. Only the ZnSe(001)//Au(111) and ZnSe(001)/Zn_1Au_0/Au(111) interfaces are thermodynamically stable within the allowed chemical potentials of Zn and Au.

The other three structures (ZnSe(001)/$Zn_{1/3}Au_{2/3}$/Au(111), ZnSe(001)/$Zn_{2/3}Au_{1/3}$/Au(111), and ZnSe(001)/Zn_0Au_1/Au(111)) are not stable at all. Actuallly, the stable ZnSe(001)/Au(111) and ZnSe(001)/Zn_1Au_0/Au(111) interfaces representing the two hybrids: The interfacing of the Se-terminated ZnSe NR end and the Zn-terminated ZnSe NR end with Au (111), respectively. Therefore, at the low chemical potential of Au (low ratio of $AuCl_3$ to ZnSe), it could only allow the Se-terminated ZnSe NR end to grow Au tips, forming the ZnSe(001)/Au(111) interface. At the increased chemical potential of Au with more added $AuCl_3$, the ZnSe(001)/Zn_1Au_0/Au(111) interface is also allowed. This agrees with experiment results that Au tips first grow on Se-terminated ZnSe(001) NRs.

2.4. Au-ZnSe hybrid NRs for photocatalytic hydrogen generation

We investigated the hydrogen evolution reaction (HER) on Au-ZnSe hybrid NRs by using the free energy of hydrogen adsorption (ΔG_{H*}, * denotes the electrode) as a single catalytic descriptor.[48] This descriptor can describe the hydrogen evolution exchange-current density.

$$i_0 = -ek_0 \frac{1}{1+\exp(-\Delta G_{H*}/kT)}$$

Where i_0 is the hydrogen evolution exchange-current density, e is the electron charge, and k_0 is a factor that needs to be fitted to experimental data. The best electrode material should have ($\Delta G_{H*} = 0$) for hydrogen evolution reaction

$$H^+ + e^- + * \rightarrow \frac{1}{2}H_2(g)$$

ΔG_{H*}, therefore, can be expressed by

$$\Delta G_{H*} = \Delta E_H + \Delta E_{ZPE} - T\Delta S_H$$

where ΔE_H, ΔE_{ZPE}, and ΔS_H are the potential energy difference, zero-point energy difference and change of entropy, respectively. At 27 °C, it can be simplified as $\Delta G_{H*} = \Delta E_H + 0.24\ eV$.[48]

The calculated HER free energies are summarized in **Table 1**. All the stable interfaces show much smaller $|\Delta G_{H*}|$ compared to the pristine Au (111) surface. This is due to the enhanced adsorption of H* by the Au atoms of interface structures. At a close look, the interface structures show an increased charge redistribution upon hydrogen adsorption as can be seen from the differential charge density plot in Figure 5c. Hydrogen adsorbed on the hybrid Au-ZnSe (Figure 5e) gains more charge than the hydrogen on pristine Au (Figure 5d). Besides the enhanced hydrogen adsorption, the unique Au-tipped NR architecture should also allow more efficient charge separation.[37] To this end, we used Au-ZnSe hybrid NRs as photocatalysts for hydrogen production through water splitting.

To reveal how the selective deposition of Au NPs on the ZnSe NRs affects their photocatalytic activities in hydrogen production, in particular to elucidate the synergistic effect of Au-ZnSe hybrid NRs, we compared photocatalytic performances of single and double Au-tipped ZnSe hybrid NRs with those of pure ZnSe NRs, Au NPs and the mixture containing both the ZnSe NRs and Au NPs (**Figure 6**a). Prior to the photocatalytic tests, phase transfer for the NPs was conducted to make them water soluble. The transfer efficiencies of NRs were measured by the element concentrations of Zn and Se elements by inductively coupled plasma-optical emission spectrometer (ICP-OES) (Table S2). As shown in Table S2, over 90% of all samples were successfully transferred to water-soluble phase and the transfer efficiencies of pure ZnSe NRs, single Au-tipped ZnSe NRs and double Au-tipped ZnSe NRs are very close to each other. The stability of Au-ZnSe hybrid NRs after phase transfer was characterized by absorption spectroscopy and TEM (Figures S11 and S12). Compared with Au-ZnSe hybrid NRs before the phase transfer, the absorption peak at 368 nm of the Au-ZnSe hybrid NRs in water became slightly broader as the surface of hybrid NRs are coated with bulky PEI ligands (Figure S11). Au-tipped ZnSe hybrid NRs were observed in the TEM image (Figure S12a) while the elongated ZnSe NRs with two tips being decorated by Au NPs were clearly seen in the corresponding STEM image (Figure S12b).

As hydrogen gas generated from the photocatalytic reaction may dissolve in the water solution, no hydrogen gas will be released to the head space of the reaction vessel until the water solution is saturated, leading to an induction time in such measurements.[10] Therefore, the hydrogen evolution rates were obtained by a linear fitting after 30 min of induction time during the 2 h illumination (Figure 6a).

As seen from Figure 6a, the hydrogen generation rate (49.8 μmol/h/g) of pure ZnSe NRs is the lowest among all NPs. This is reasonable because the recombination rate of light-induced electrons and holes in pure ZnSe NRs is relatively high.[49] In contrast, pure Au NPs with a diameter of 5.56 nm present a higher hydrogen generation rate of 149.9 μmol/h/g. Extinction spectrum of the Au NPs shows a broad plasmon resonance peak at 520 nm (Figure S13). It is expected that the plasmon resonance induced hot electrons in Au NPs may lead to water reduction for hydrogen production.[50-52] The mixture of Au NPs and ZnSe NRs show a lower hydrogen generation rate of 51.5 μmol/h/g compared with that of pure Au NPs (Figure 6a). In the physically mixed sample, the concentration of Au NPs, and hence the plasmon resonance centres, in the water solution is reduced, this decreases the generation of hot reductive electrons, leading to a lower hydrogen generation rate, as compared with pure Au NP sample. Furthermore, because ZnSe NRs have a large absorption cross-section, [36] the incorporation of ZnSe NRs with Au NPs in the water solution can intervene the light absorption of Au NPs and then dampen their plasmon resonance, affecting the generation of hot electrons.

Rather than physically mixing the Au NPs and ZnSe NRs, we have selectively deposited Au NPs on ZnSe NRs, constituting single and double Au-tipped ZnSe hybrid NRs (Figure 3). In such a hybrid structure, electron-hole pairs are generated by the light absorption of ZnSe NRs, and are further effectively separated on the metal-semiconductor heterojuncitons, which allows it to act as a photocatalyst to catalyze the redox reaction for hydrogen production via water splitting. As depicted in Figure 6a, single Au-tipped ZnSe hybrid NRs are more

efficient (~437.8 μmol/h/g) in hydrogen generation than double Au-tipped ZnSe hybrid NRs (~325.1 μmol/h/g). In the single Au-tipped ZnSe hybrid NRs, the direct contact of other end of the ZnSe NRs with the solution make it conducive to the hole transfer and consumption by a scavenger after the electron transfer to the Au tip. In the double Au-tipped ZnSe hybrid NRs, the light-induced holes can only be transferred to the scavenger through the less active, defect-free and surfactant passivated side facets, which reduces the efficiency of hole clearance and therefore consequently reduced the hydrogen generation rate.[39,53-54] The apparent quantum efficiency (AQE) under irradiation for single Au-tipped ZnSe hybrid NRs was measured to be approximately 1.3% (λ=365 nm) (See Supporting Information for details).

It is noteworthy that Au-tipped ZnSe hybrid NRs only show weak plasmon resonance due to the tiny size of the Au domain. Furthermore, as demonstrated in the control experiment, ZnSe NRs can intervene the light absorption of Au NPs which reduces the photocatalytic performance of Au NPs in hydrogen generation. Therefore, the good photocatalytic properties of Au-tipped ZnSe hybrid NRs are mainly attributed to the efficient charge separation enabled by the metal-semiconductor heterojunctions, where Au NPs work as the electron sink to efficiently accept/trap electrons.[55] The plasmon resonance induced hot electron transfer in Au-tipped ZnSe hybrid NRs contributes to the photocatalytic activities only to a small extent due to its tiny size.[56-57]

In order to further verify the photocatalytic mechanism, we compared the photoluminescence spectrum (Figure S14) and photocurrent (Figure 6b) of Au-ZnSe hybrid NRs with that of pure ZnSe NRs. To test photoluminescence spectrum, we have performed surface ligand exchange by using trioctylphosphine (TOP) to ensure Au-ZnSe hybrid NRs and pure ZnSe NRs have same surface conditions. As depicted in Figure S14, the Au-ZnSe coated with either DDT + OLA or TOP shows significantly reduced photoluminescence intensities compared with ZnSe NRs with similar surface conditions. The quenching effect of the photoluminescence can be attributed to the reduced radiative recombination rates induced by

the charge separation by the heterojunction between Au tips and ZnSe NRs in the hybrid NRs.[39]

The photocurrent testing was also performed to study the photocatalytic mechanism (Figure 6b). As shown in Figure 6b, single Au-tipped ZnSe hybrid NRs show the highest photocurrent of 87.9 nA/cm^2. Even the photocurrent of double Au-tipped-ZnSe hybrid NRs (83.3 nA/cm^2) is slightly lower than that of single Au-tipped ZnSe hybrid NRs, it is ~1.4 times higher than that of pure ZnSe NRs (60.1 nA/cm^2). These results are consistent with the hydrogen generation rate results shown in Figure 6a, which confirmed the effective electron transfer after photoexcitation in Au-tipped ZnSe hybrid NRs.

Based on above results, we depict the photocatalytic mechanism of Au-ZnSe hybrid NRs in Figure 6c and 6d. Upon illumination, excited electrons at the bottom of the conduction band of ZnSe will transfer to Au domain because the Fermi level of Au is lower than the bottom of the conduction band of ZnSe[26,58-60]. The induced holes will stay in the valence band, and thus the electrons and holes are effectively and spatially separated and the probability for recombination is greatly reduced. Rich in electrons, the Au tips with enhanced capture ability of H can efficiently catalyze proton reduction and hydrogen production while the holes (h^+) in ZnSe NRs are removed by introduction of hole scavengers i.e. methanol (Figure 6d).

3. Conclusion

Novel Au-ZnSe hybrid NRs with controlled size and site selectivity of Au tips have been synthesized using wet-chemical approaches. Au atoms grew non-epitaxially on ZnSe NRs. Au tips growth on ZnSe hybrid NRs show enhanced hydrogen adsorption that improves the HER catalytic properties, and photocatalytic hydrogen production rate of 437.8 μmol·h^{-1}·g^{-1} and a APE of 1.3% was obtained by using methanol as sacrificial hole scavenger. Due to the tiny size of Au tips, plasmon resonance induced hot electron transfer in Au-tipped ZnSe hybrid NRs contributes to the photocatalytic activities only to a small extent as most of electron-holes pairs are generated from ZnSe semiconductor NRs. It is worth noting that Au

tipped ZnSe hybrid NRs can only absorb UV and blue ranges of the solar spectrum. Further expanding their absorption from blue to visible spectral range through hetero-semiconductors and/or doping aforementioned to realize the full potential of metal-semiconductor hybrid NPs for solar energy application is of significant importance. Furthermore, we anticipate the photocatalytic performances of Au-ZnSe hybrid NRs can be further improved by optimizing the size and type of noble metal species (e.g. Pt or alloyed Au-Pt) as well as number of noble metal domains on the NRs. This work opens an avenue for new Cd-free metal-semiconductor hybrid NP-based photocatalysis for hydrogen generation by water splitting, with relevance to redox reactions in biochemistry.

Supporting Information
Supporting Information is available from the Wiley Online Library or from the author.

Acknowledgements

W.C. and X.L contributed equally to this work. This work was supported by Australian Research Council (ARC) Discovery Early Career Researcher Award (DECRA) (DE 160100589) and discovery project (DP 170104264). Y. Li acknowledges support from the NSFC (grant no. 11674131). W.C. acknowledged the scholarship from the China Scholarship Council. The authors acknowledge Kelly Merigot, Zakaria Quadir, Veronica Avery and Jean-Pierre Veder from the John de Laeter Research Centre for Microscopy, Characterization & Analysis Curtin University, Australia for technical assistance in TEM, XRD, and XPS characterizations, respectively. The authors acknowledge Yijun Zhong from Department of Chemical Engineering, Curtin University for experimental assistance.

Received: ((will be filled in by the editorial staff))
Revised: ((will be filled in by the editorial staff))
Published online: ((will be filled in by the editorial staff))

References

[1] T. Mokari, E. Rothenberg, I. Popov, R. Costi, U. Banin, *Science* **2004**, *304*, 1787.

[2] H. Schlicke, D. Ghosh, L.-K. Fong, H. L. Xin, H. Zheng, A. P. Alivisatos, *Angew. Chem. Int. Ed.* **2013**, *52*, 980.

[3] S. E. Habas, P. Yang, T. Mokari, *J. Am. Chem. Soc.* **2008**, *130*, 3294.

[4] Z. Han, F. Qiu, R. Eisenberg, P. L. Holland, T. D. Krauss, *Science* **2012**, *338*, 1321.

[5] J. Zhang, Y. Tang, K. Lee, M. Ouyang, *Nature* **2010**, *466*, 91.

[6] J. Zhang, Y. Tang, K. Lee, M. Ouyang, *Science* **2010**, *327*, 1634.

[7] P. D. Cozzoli, T. Pellegrino, L. Manna, *Chem. Soc. Rev.* **2006**, *35*, 1195.

[8] a) D. Chen, H. Zhang, Y. Li, Y. Pang, Z. Yin, H. Sun, L. C. Zhang, S. Wang, M. Saunders, E. Barker, G. Jia, *Adv. Mater.* **2018**, *30*, 1803351; b) S. Javaid, Y. Li, D. Chen, X. Xu, Y. Pang, W. Chen, F. Wang, Z. Shao, M. Saunders, J. P. Veder, G. Jia, F. Jones, *J. Phys. Chem. C.* **2019**, *123*, 10604.

[9] Y. Ben-Shahar, F. Scotognella, I. Kriegel, L. Moretti, G. Cerullo, E. Rabani, U. Banin, *Nat. Commun.* **2016**, *7*, 10413.

[10] Y. Ben-Shahar, F. Scotognella, N. Waiskopf, I. Kriegel, S. Dal Conte, G. Cerullo, U. Banin, *Small* **2015**, *11*, 462.

[11] Q. Q. Bi, J. W. Wang, J. X. Lv, J. Wang, W. Zhang, T. B. Lu, *ACS Catal.* **2018**, *8*, 11815.

[12] N. Waiskopf, Y. Ben-Shahar, M. Galchenko, I. Carmel, G. Moshitzky, H. Soreq, U. Banin, *Nano Lett.* **2016**, *16*, 4266.

[13] J. X. Fan, M. D. Liu, C. X. Li, S. Hong, D. W. Zheng, X. H. Liu, S. Chen, H. Cheng, X. Z. Zhang, *Nanoscale Horiz.* **2017**, *2*, 349.

[14] C. Mao, Y. Xiang, X. Liu, Z. Cui, X. Yang, K. W. K. Yeung, H. Pan, X. Wang, P. K. Chu, S. Wu, *ACS Nano* **2017**, *11*, 9010.

[15] Y. Zhang, X. Liu, Z. Li, S. Zhu, X. Yuan, Z. Cui, X. Yang, P. K. Chu, S. Wu, *ACS Appl. Mater. Interfaces* **2018**, *10*, 1266.

[16] A. A. Pawar, S. Halivni, N. Waiskopf, Y. Ben-Shahar, M. Soreni-Harari, S. Bergbreiter, U. Banin, S. Magdassi, *Nano Lett.* **2017**, *17*, 4497.

[17] A. Figuerola, M. van Huis, M. Zanella, A. Genovese, S. Marras, A. Falqui, H. W. Zandbergen, R. Cingolani, L. Manna, *Nano Lett.* **2010**, *10*, 3028.

[18] S. Naskar, A. Schlosser, J. F. Miethe, F. Steinbach, A. Feldhoff, N. C. Bigall, *Chem. Mater.* **2015**, *27*, 3159.

[19] M. A. van Huis, A. Figuerola, C. Fang, A. Beche, H. W. Zandbergen, L. Manna, *Nano Lett.* **2011**, *11*, 4555.

[20] K. Wu, Z. Chen, H. Lv, H. Zhu, C. L. Hill, T. Lian, *J. Am. Chem. Soc.* **2014**, *136*, 7708.

[21] T. Simon, N. Bouchonville, M. J. Berr, A. Vaneski, A. Adrovic, D. Volbers, R. Wyrwich, M. Doblinger, A. S. Susha, A. L. Rogach, F. Jackel, J. K. Stolarczyk, J. Feldmann, *Nat. Mater.* **2014**, *13*, 1013.

[22] L. Ma, K. Chen, F. Nan, J. H. Wang, D. J. Yang, L. Zhou, Q. Q. Wang, *Adv. Funct. Mater.* **2016**, *26*, 6076.

[23] L. Amirav, A. P. Alivisatos, *J. Phys. Chem. Lett.* **2010**, *1*, 1051.

[24] S. Linic, P. Christopher, D. B. Ingram, *Nat. Mater.* **2011**, *10*, 911.

[25] C. M. Wolff, P. D. Frischmann, M. Schulze, B. J. Bohn, R. Wein, P. Livadas, M. T. Carlson, F. Jäckel, J. Feldmann, F. Würthner, J. K. Stolarczyk, *Nat. Energy.* **2018**, *3*, 862.

[26] X. Xiang, L. Chou, X. Li, *Chin. J. Cata* **2018**, *39*, 407.

[27] P. Kalisman, L. Houben, E. Aronovitch, Y. Kauffmann, M. Bar-Sadan, L. Amirav, *J. Phys. Chem. A* **2015**, *3*, 19679.

[28] B. Zhou, J. Song, C. Xie, C. Chen, Q. Qian, B. Han, *ACS Sustainable Chem. Eng.* **2018**, *6*, 5754.

[29] Y. Shemesh, J. E. Macdonald, G. Menagen, U. Banin, *Angew. Chem. Int. Ed.* **2011**, *50*, 1185.

[30] B. A. Rzigalinski, J. S. Strobl, *Toxicol. Appl. Pharmacol.* **2009**, *238*, 280.

[31] R. F. Domingos, D. F. Simon, C. Hauser, K. J. Wilkinson, *Environ. Sci. Technol.* **2011**, *45*, 7664.

[32] Z. Wu, W. Wang, Y. Cao, J. He, Q. Luo, W. A. Bhutto, S. Li, J. Kang, *J. Mater. Chem. A* **2014**, *2*, 14571.

[33] T. T. Zhuang, Y. Liu, Y. Li, Y. Zhao, L. Wu, J. Jiang, S. H. Yu, *Angew. Chem. Int. Ed. Engl*. **2016**, *55*, 6396.

[34] M. F. Kuehnel, C. E. Creissen, C. D. Sahm, D. Wielend, A. Schlosser, K. L. Orchard, E. Reisner, *Angew. Chem. Int. Ed.* **2019**, *58*, 5059.

[35] G. Jia, Y. Pang, J. Ning, U. Banin, B. Ji, *Adv. Mater.* **2019**, 31, 1900781.

[36] a) G. Jia, U. Banin, *J. Am. Chem. Soc.* **2014**, *136*, 11121; b) W. Chen, A. Karton, T. Hussian, S. Javaid, F. Wang, Y. Pang, G. Jia, *CrystEngComm* **2019**, *21*, 2955; c) D. Chen, A. Wang, H. Li, L. Abad Galan, C. Su, Z. Yin, M. Massi, A. Suvorova, M. Saunders, J. Li, A. Sitt, G. Jia, *Nanoscale* **2019**, *11*, 10190; d)Y. Pang, M. Zhang, D. Chen, W. Chen, F. Wang, S. J. Anwar, M. Saunders, M. R. Rowles, L. Liu, S. Liu, A. Sitt, C. Li, G. Jia, *J. Phys. Chem. Lett.* **2019**, *10*, 3465.

[37] R. Bose, A. H. Wasey, G. P. Das, N. Pradhan, *J. Phys. Chem. Lett.* **2014**, *5*, 1892.

[38] a) J. Selvaraj, A. Mahesh, V. Asokan, V. Baskaralingam, A. Dhayalan, T. Paramasivam, *ACS Appl. Nano Mater.* **2017**, *1*, 371; b) S.-H. Chang, M.-Y. Chiang, C.-C. Chiang, F.-W. Yuan, C.-Y. Chen, B.-C. Chiu, T.-L. Kao, C.-H. Lai, H.-Y. Tuan, *Energy Environ. Sci.* **2011**, *4*, 4929; c) M-C. Bourg, A. Badia, R. B. Lennox, *J. Phys. Chem. B* **2000**, *104*, 6562.

[39] a) J. U. Bang, S. J. Lee, J. S. Jang, W. Choi, H. Song, *J. Phys. Chem. Lett.* **2012**, *3*, 3781; b) E. Shaviv, O. Schubert, M. Alves-Santos, G. Goldoni, R. D. Felice, F. Vallee, N. D. Fatti, U. Banin, C. Sonnichsen, *ACS Nano* **2011**, *5*, 4712. c) J. B. ten Hove, L. M. I. Schijven, J. Wang, A. H. Velders, *Chem. Commun*. **2018**, *54*, 13355.

[40] a) T. Mokari, C. G. Sztrum, A. Salant, E. Rabani, U. Banin, *Nat. Mater.* **2005**, *4*, 855.S. b) Chakrabortty, J. A. Yang, Y. M. Tan, N. Mishra, Y. Chan, *Angew. Chem. Int. Ed.* **2010**, *49*, 2888.

[41] R. Costi, A. E. Saunders, U. Banin, *Angew. Chem. Int. Ed.* **2010**, *49*, 4878.

[42] G. Pramanik, J. Humpolickova, J. Valenta, P. Kundu, S. Bals, P. Bour, M. Dracinsky, P. Cigler, *Nanoscale* **2018**, *10*, 3792.

[43] A. Villa, N. Dimitratos, C. E. Chan-Thaw, C. Hammond, G. M. Veith, D. Wang, M. Manzoli, L. Prati, G. J. Hutchings, *Chem. Soc. Rev.* **2016**, *45*, 4953.

[44] B. Canava, J. Vigneron, A. Etcheberry, J. F. Guillemoles, D. Lincot, *Appl. Surf. Sci*. **2002**, *202*, 8.

[45] E. New, I. Hancox, L. A. Rochford, M. Walker, C. A. Dearden, C. F. McConville, T. S. Jones, *J. Mater. Chem. A* **2014**, *2*, 19201.

[46] A. R. Noble-Luginbuhl, R. G. Nuzzo, *Langmuir* **2001**, *17*, 3937.

[47] K. K. Haldar, N. Pradhan, A. Patra, *Small* **2013**, *9*, 3424.

[48] J. K. Nørskov, T. Bligaard, A. Logadottir, J. R. Kitchin, J. G. Chen; S. Pandelov, U. Stimming, *J. Electrochem. Soc.* **2005**, *152*, 23.

[49] K. Wu, T. Lian, *Chem. Soc. Rev.* **2016**, *45*, 3781.

[50] Z. Liu, Z. Lu, M. Bosman, N. Li, T. J. Frankcombe, G. Jia, A. Tricoli, Y. Liu, Y. Du, Z. Yin, *Small* **2018**, *14*, 1803233.

[51] Z. Lou, M. Fujitsuka, T. Majima, *ACS Nano* **2016**, *10*, 6299.

[52] L. Liu, X. Zhang, L. Yang, L. Ren, D. Wang, J. Ye, *Natl. Sci. Rev.* **2017**, *4*, 761.

[53] Y. Nakibli, P. Kalisman, L. Amirav, *J. Phys. Chem. Lett.* **2015**, *6*, 2265.

[54] T. Simon, M. T. Carlson, J. K. Stolarczyk, J. Feldmann, *ACS Energy Lett.* **2016**, *1*, 1137.

[55] a)V. Subramanian, E. E. Wolf, P. V. Kamat, *J. Am. Chem. Soc.* **2004**, *126*, 4943; b) M. Murdoch, G. Waterhouse, M. Nadeem, J. Metson, M. Keane, R. Howe, J. Llorca, H. Idriss, *Nat. Chem.* **2011**, *3*, 489; c) Z. Yin, B. Chen, M. Bosman, X. Cao, J. Chen, B. Zheng, H. Zhang, *Small* **2014**, 10, *17*, 3537.

[56] a) J. A. Scholl, A. L. Koh, J. A. Dionne, *Nature* **2012**, *483*, 421; b) K. Wu, W. E. Rodriguez-Cordoba, Y. Yang, T. Lian, *Nano Lett.* **2013**, *13*, 5255.

[57] M. Zhou, C. Zeng, Y. Chen, S. Zhao, M. Y. Sfeir, M. Zhu, R. Jin, *Nat. Commun.* **2016**, *7*, 13240.

[58] N. Oh, S. Nam, Y. Zhai, K. Deshpande, P. Trefonas, M. Shim, *Nat. Commun.* **2014**, *5*, 3642.

[59] A. Wang, H. Shen, S. Zang, Q. Lin, H. Wang, L. Qian, J. Niu, L. S. Li, *Nanoscale* **2015**, *7*, 2951.

[60] J. Zhou, H. L. Zhuang, H. Wang, *Nanoscale* **2017**, *9*, 17303.

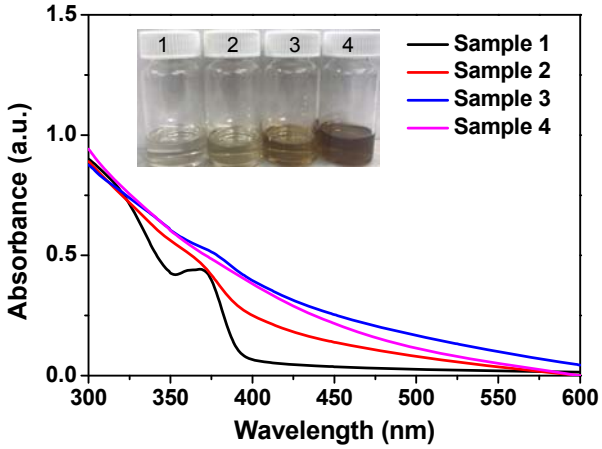

Figure 1. Comparison of UV-Vis absorption spectra of Au-ZnSe hybrid NRs obtained by using different molar ratios of Au precursor to ZnSe NRs. (1) n(Au: ZnSe NRs) =127:1; (2) n(Au:ZnSe NRs) =254:1; (3) n(Au:ZnSe NRs) =762:1; (4) n(Au:ZnSe NRs) =1270:1. Inset shows a photograph of Au-ZnSe hybrid NRs dispersed in toluene solution.

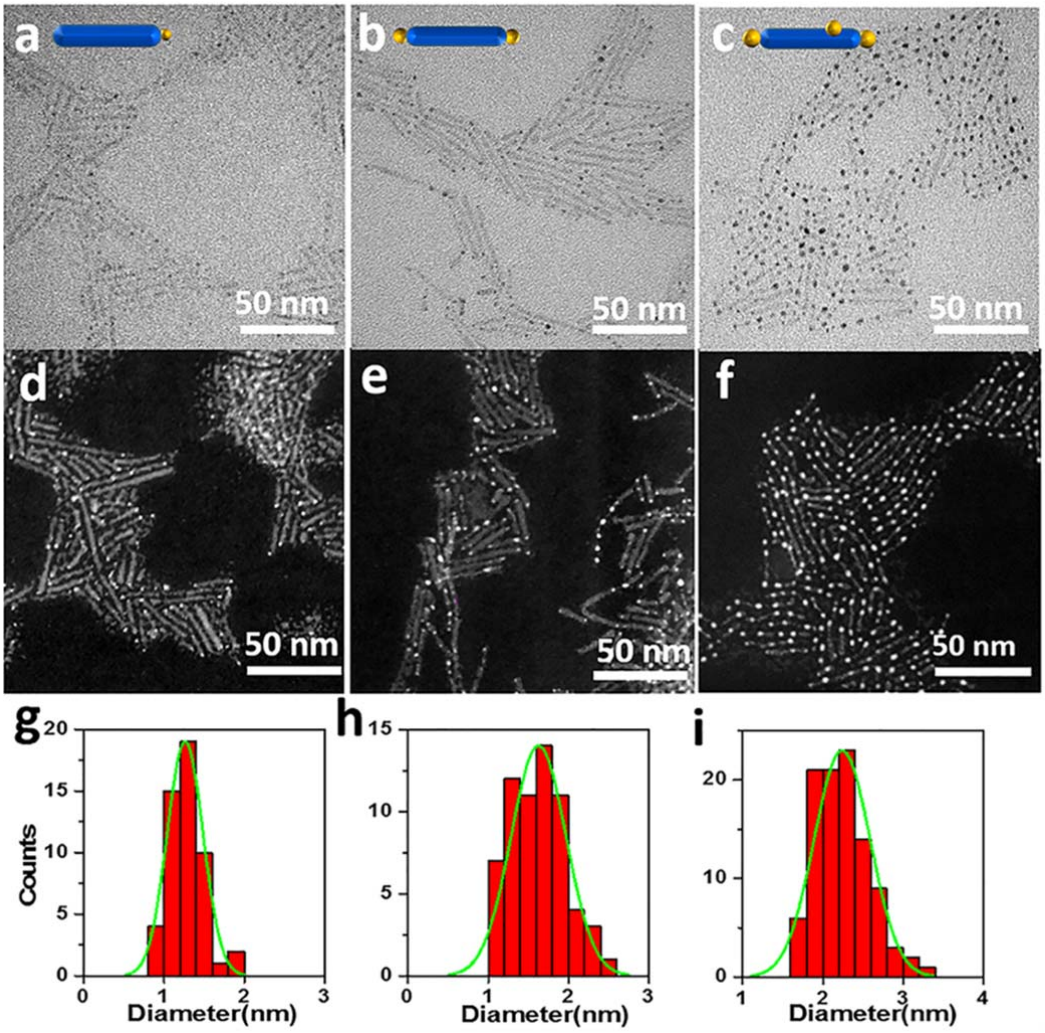

Figure 2. TEM images of Au-ZnSe hybrid NRs with Au tips of variable size. (a) 1.3 ± 0.2 nm (Sample 2 in Figure 1); (b) 1.6 ± 0.3 nm (Sample 3 in Figure 1); (c) 2.2 ± 0.3 nm (Sample 4 in Figure 1). (d-e) STEM images corresponding to (a-c). (g-i) Particle size histograms corresponding to (a-c).

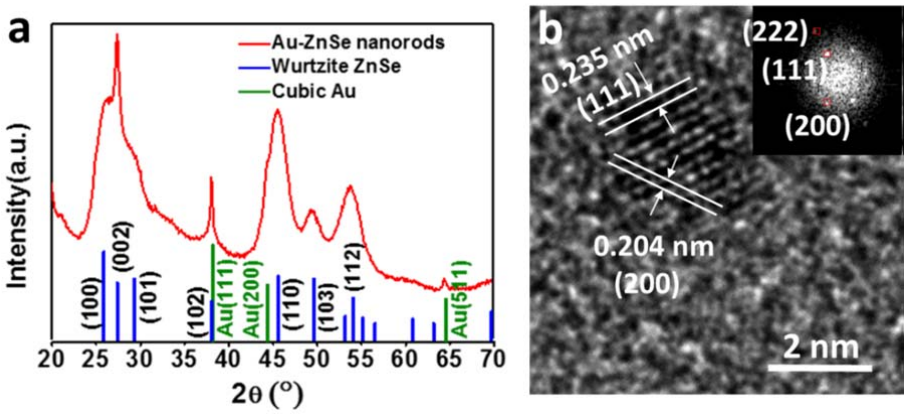

Figure 3. (a) XRD pattern, (b) HRTEM image of Au-ZnSe hybrid NRs (Inset shows the corresponding FFT image).

1

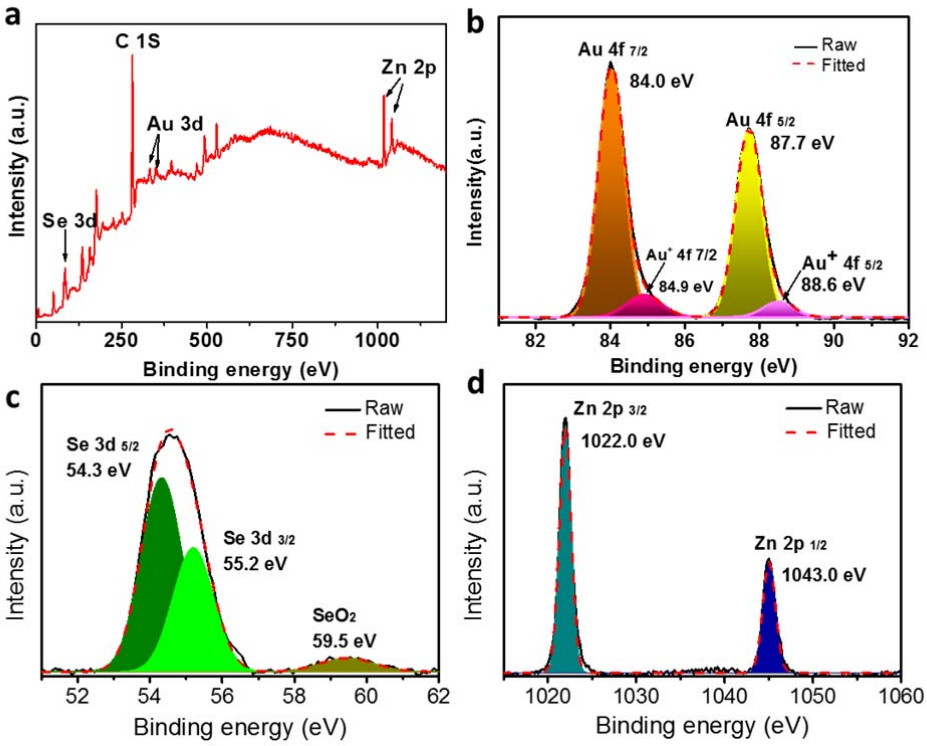

2

3 **Figure 4.** XPS spectra of the Au-ZnSe hybrid NRs. (a) Survey spectrum, (b-d) Binding

4 energy peaks of (b) Au 4f, (c) Se 3d and (d) Zn 2p.

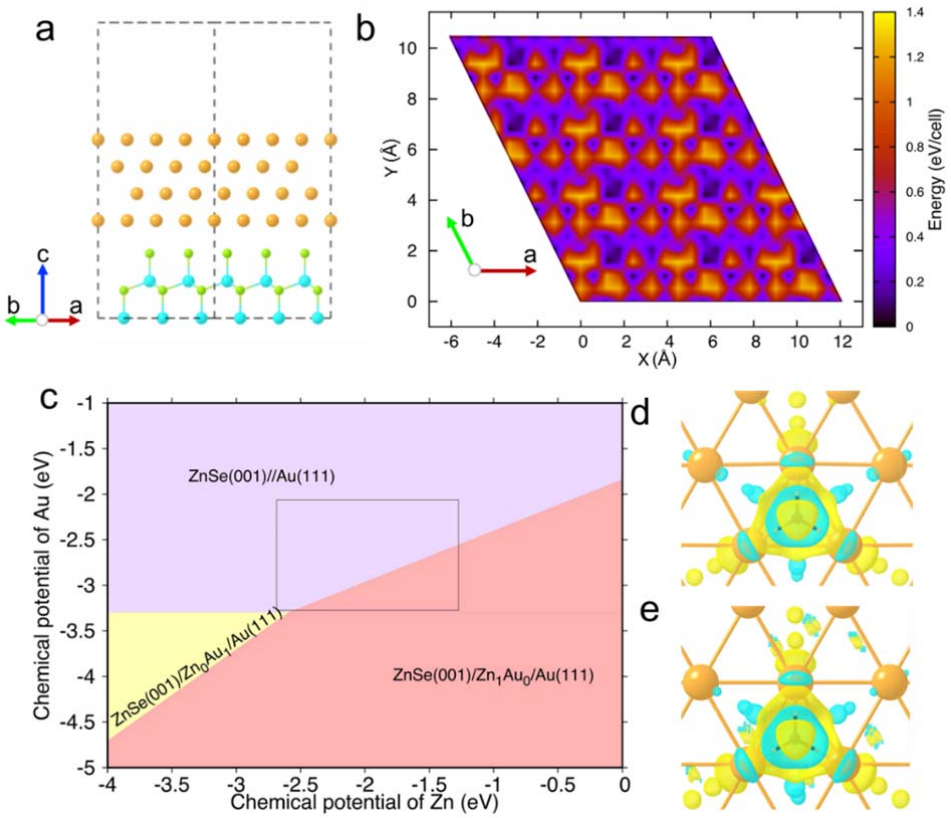

Figure 5. (a) Initial input interface structure for potential energy surface calculations of ZnSe(001)/Au(111) interface, which contains 64 Au atoms, 18 Zn atoms and 18 Se atoms; (b) Calculated potential energy surface of ZnSe(001)/Au(111) interface. (c) Phase diagram of ZnSe (001)/Au (111) interface. Five structures were explored, namely, the ZnSe(001)/Au(111), ZnSe (001)/Zn_0Au_1 /Au(111), ZnSe (001)/$Zn_{1/3}Au_{2/3}$ /Au (111), ZnSe(001)/$Zn_{2/3}Au_{1/3}$/Au(111), and ZnSe(001)/Zn_1Au_0/Au(111). The ZnSe(001)/$Zn_{1/3}Au_{2/3}$/Au(111) and ZnSe(001)/$Zn_{2/3}Au_{1/3}$/Au(111) interfaces are not thermodynamically stable. The inset rectangular represents the allowed chemical potentials of Zn and Au. The chemical potential of Zn is bounded by $\mu_{ZnSe} - \mu_{Se} < \mu_{Zn} < \mu_{hcp-Zn}$, and the chemical potential of Au is bounded by $\mu_{fcc-Au} < \mu_{Au} < \mu_{AuSe} + \mu_{Zn} - \mu_{ZnSe}$. Differential charge density diagrams for hydrogen adsorption onto a fcc site of pristine Au (111) (d) and top Au (111) of ZnSe(001)//Au(111) interface (e). Golden and black balls

1 indicate the Au and H atoms, respectively. Yellow and cyan indicate the charge loss and gain,
2 respectively. Isosurface value is 0.001 e/Å^3.

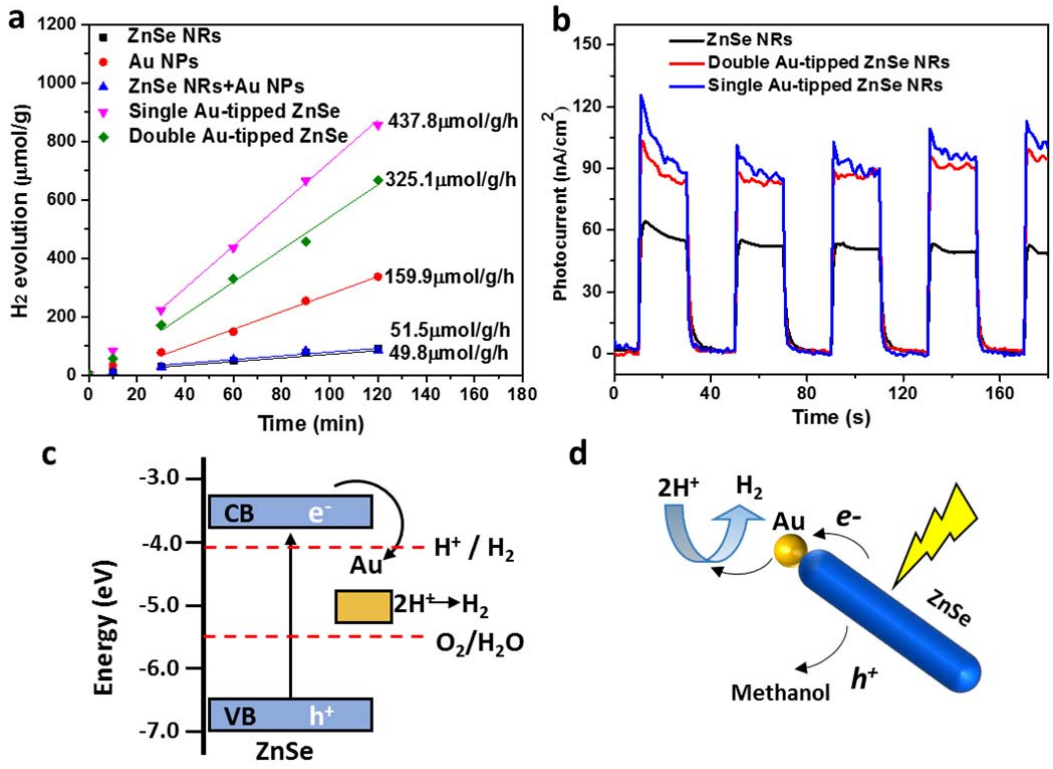

Figure 6. (a) Comparison of hydrogen generation rates of pure ZnSe NRs, Au NPs, single Au-tipped Au-ZnSe hybrid NRs and double Au-tipped ZnSe hybrid NRs using methanol as the sacrificial hole scavenger. (b) Transient photocurrent with different working electrodes, i.e. pure ZnSe NRs, single Au-tipped ZnSe and double Au-tipped ZnSe hybrid NRs. (c) Energy band alignment diagram of Au-ZnSe hybrid NRs; (d) Proposed photocatalytic mechanism of Au-ZnSe hybrid NRs for hydrogen production in water splitting.

Table 1. Calculated free energy change for hydrogen evolution on different electrodes.

Electrode	$\|\Delta G_{H*}\|$ **(eV)**	
	fcc site	*hcp* site
Au (111)	0.38	0.43
ZnSe(001)//Au(111)	0.28	0.27
ZnSe(001)/Zn_1Au_0/Au(111)	0.15	0.24
ZnSe(001)/Zn_0Au_1/Au(111)	0.10	0.26

The table of contents entry:

Au-ZnSe hybrid nanorods with controlled size and location of Au domains are synthesized and tested for hydrogen production by photocatalytic water splitting for the first time. The non-epitaxial growth of Au tips on ZnSe NRs is studied experimentally and theoretically. This new Cd-free hybrid system may provide a platform for hybrid NP-based photocatalysis towards clean fuel production.

Keyword: Au-ZnSe, hybrid nanorods, cadmium-free, hydrogen production, photocatalysis

Wei Chen, Xiaojie Li, Fei Wang, Shaghraf Javaid, Yingping Pang, Jiayi Chen, Zongyou Yin, Shaobin Wang*, Yunguo Li*, Guohua Jia*

Title:

Non-Epitaxial Gold-Tipped ZnSe Hybrid Nanorods for Efficient Photocatalytic Hydrogen Production